Technical Notes

TECHNICAL NOTES are short manuscripts describing new developments or important results of a preliminary nature. These Notes cannot exceed 6 manuscript pages and 3 figures; a page of text may be substituted for a figure and vice versa. After informal review by the editors, they may be published within a few months of the date of receipt. Style requirements are the same as for regular contributions (see inside back cover).

Propeller Design by Optimization

Magdi H. Rizk* and Wen-Huei Jou†
Flow Research Company, Kent, Washington

Introduction

A RESURGENCE of interest in recent years in the turboprop propulsion system has been caused by the projected high fuel costs in the 1990s and the potential savings in fuel consumption that can be achieved with such a propulsion system. Advance propellers operate at transonic speeds. Therefore, one of the two basic elements required for optimizing the design of these propellers is an analysis code capable of solving the nonlinear flow equations about the propeller so that the compressibility effects are predicted. The second element is an optimization scheme that can be efficiently combined with the analysis code. Recent procedures[1,2] for designing propellers combine vortex lattice aerodynamic analysis with standard optimization procedures. Our goal is to develop an efficient procedure for optimizing the design of advanced propellers. The present preliminary work is a step toward achieving that goal.

A preliminary design code has been developed. The basis of this code is the finite volume code developed by Jou[3] for solving the potential flow about a propeller by line relaxation. This code calculates the transonic flowfield about propellers. Optimizing propeller design in this flow regime is our ultimate goal. However, in this initial phase of the investigation, we have limited all computations to subsonic ($M_\infty \simeq 0$) flow calculations. The analysis code is combined with the single-cycle optimization approach[4,5] to produce an efficient design code.

Approach

For a lightly loaded propeller with a large number of blades, the optimum condition for maximum efficiency η is obtained when the sectional efficiency distribution η_s along the blade is constant.[6] Minimizing the objective function E, where

$$E=\int_{r_h}^{r_t}(\eta_s-\bar{\eta})^2 dr \qquad \bar{\eta}=\frac{1}{r_t-r_h}\int_{r_h}^{r_t}\eta_s dr$$

and r_h and r_t are, respectively, the hub and tip radii normalized by the propeller diameter, results in a sectional efficiency distribution that is nearly constant. This objective function is minimized, subject to the constraint of a specified propeller power coefficient C_P. The vector of design parameters $\boldsymbol{P}=(P_1, P_2, P_3)$ defines the blade sectional angle-of-attack distribution α (see Fig. 1), as follows:

$$\alpha=P_1+P_2\frac{r-r_a}{r_t-r_h}+P_3\frac{r^2-r_b^2}{(r_t-r_h)^2}$$

where r_a and r_b are chosen so that the integrals of the linear and quadratic terms along the blade are zero.

Traditional optimization methods (e.g., the steepest descent method and the conjugate gradient method) are iterative procedures that require the evaluation of the objective function many times before the converged optimum solution is determined. Since E is dependent on the potential function ϕ in addition to $\boldsymbol{P}$, the flow governing equation must be solved each time E is evaluated. Therefore, any of the traditional optimization schemes become two-cycle (inner-outer) iterative procedures. The inner iterative cycle solves the analysis problem for ϕ iteratively, while the outer cycle determines the optimum $\boldsymbol{P}$ iteratively. This costly procedure is replaced here by the single-cycle approach, which modifies the iterative procedure for solving the flow governing equation so that ϕ and $\boldsymbol{P}$ are updated simultaneously. Thus, the need for the costly inner-outer iterative procedure is eliminated. Details of this procedure are given in Refs. 4, 5, and 7.

Results

An example for a propeller with four straight blades is computed. Each blade has a constant chord NACA 0008 section at an aspect ratio of 5 mounted on a cylinder with a radius of 16% of the span. The forward Mach number is 0.1 and the advance ratio J is 3.06. The constraint on the power coefficient is given by $C_P=0.7$.

Calculations are initially performed on a coarse mesh ($18\times12\times8$) (x, y, r) with the initial perturbation velocity potential set equal to zero. The resulting solutions are used as an initial guess for the medium mesh ($36\times24\times16$) calculation, which is followed by the fine mesh ($72\times48\times32$) calculation.

The evolution histories of the design parameters are shown in Fig. 2. The evolution histories of the power and efficiency are shown in Fig. 3. From Figs. 2 and 3, two distinct stages in the convergence process of the design parameters may be identified for each of the meshes. In the first stage, relatively rapid changes in the values of $\boldsymbol{P}$, C_P, and η occur as they approach

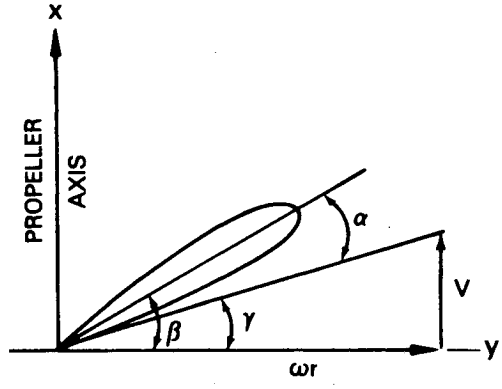

Fig. 1 Propeller blade section.

Submitted July 18, 1985; revision submitted Jan. 27, 1986.

*Program Manager, Aerodynamics, Applied Mechanics Division. Member AIAA.
†Vice President, Applied Mechanics Division. Member AIAA.

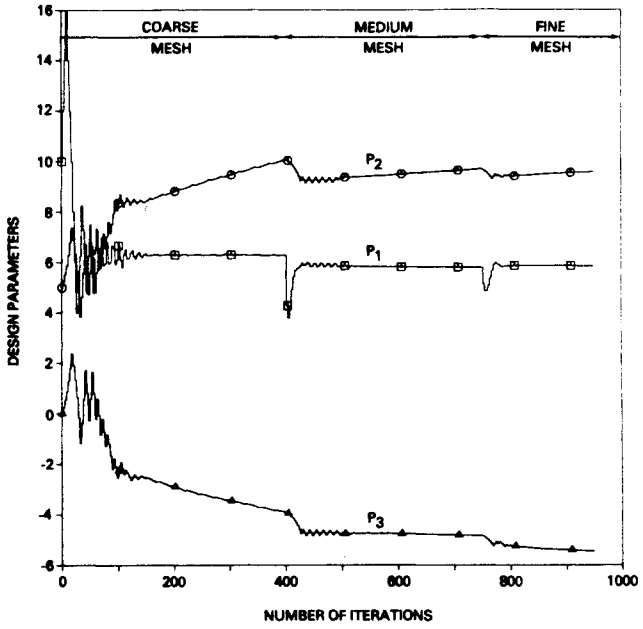

Fig. 2 Design parameters evolution histories.

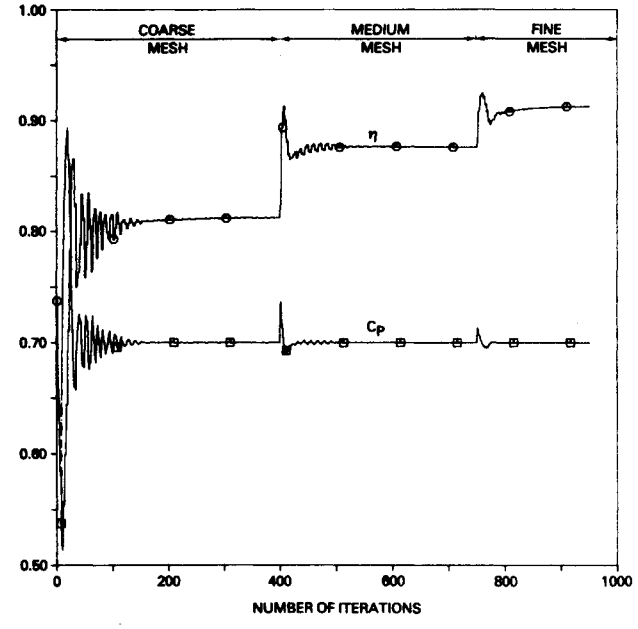

Fig. 3 Power and efficiency evolution histories.

the converged values of the solutions. At the end of this stage, these parameters are close to their final values. In the second stage, minor adjustments take place as the parameter values converge to their final values.

The maximum residual R, which is a measure of the convergence of the flow field solution ϕ, is shown in Fig. 4a. The high-frequency oscillations apparent in the figure are due to the introduction of a perturbation in the boundary conditions as P is updated. The corresponding R curve for the analysis problem is shown in Fig. 4b. Comparison of these two figures indicates that the rate of convergence in both the design and analysis problems is about the same. However, on the average, the iterative step in the design problem is more costly than that for the analysis problem. The ratio of the computation cost for the design problem to that for the analysis problem is found to be 2.43.

The angle of attack, sectional efficiency, and power distributions along the blade are shown in Fig. 5. As indicated, our

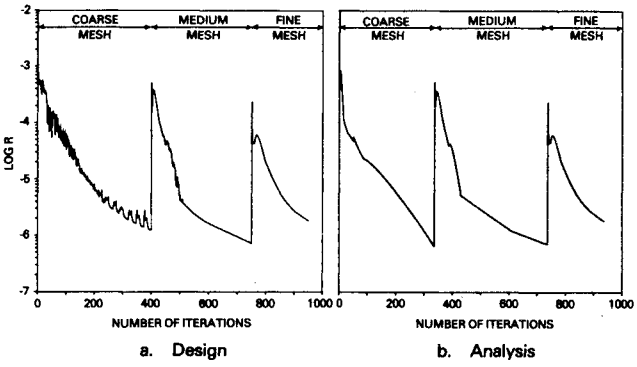

Fig. 4 Residual evolution history.

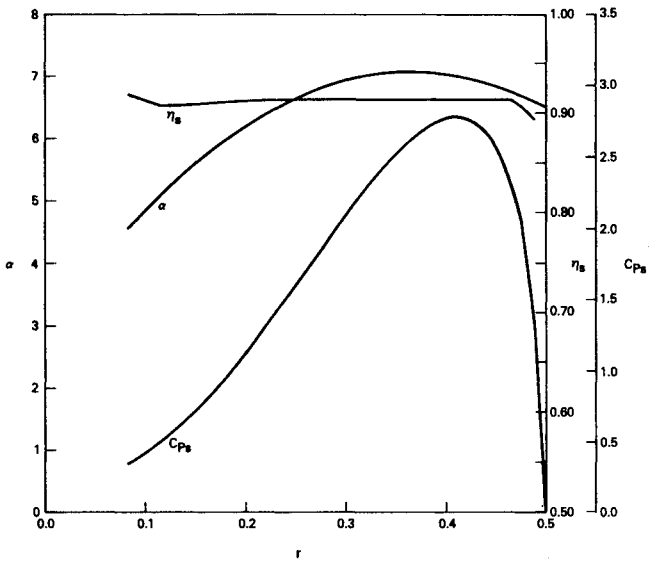

Fig. 5 Sectional angle of attack, sectional efficiency, and sectional power distributions along the blade.

objective of determining a blade twist distribution, which results in a uniform sectional efficiency distribution along the blade, has been achieved.

Conclusions

In this study, we have investigated and demonstrated the feasibility of combining an analysis code and an optimization procedure for designing propellers. The present work is a step toward achieving the goal of developing an efficient procedure for optimizing the design of advanced propellers. To achieve that goal, the present objective function must be replaced by a more accurate one and calculations must be performed at higher Mach numbers.

Acknowledgment

This work was sponsored by NASA Lewis Research Center under Contract NAS3-24533.

References

[1]Chang, L. K. and Sullivan, J. P., "Optimization of Propeller Blade Twist by an Analytical Method," *AIAA Journal*, Vol. 22, Feb. 1984, pp. 252-255.

[2]Miller, C. J. and Sullivan, J. P., "Noise Constraints Effecting Optimal Propeller Designs," SAE Paper 850871, April 1985.

[3]Jou, W.-H., "Finite Volume Calculation of Three-Dimensional Flow around a Propeller," *AIAA Journal,* Vol. 21, Oct. 1983, pp. 1360-1364.

[4]Rizk, M. H., "The Single-Cycle Scheme: A New Approach to Numerical Optimization," *AIAA Journal,* Vol. 21, Dec. 1983, pp. 1640-1647.

[5]Rizk, M. H., "Application of the Single-Cycle Optimization Approach to Aerodynamic Design," *Journal of Aircraft*, Vol. 22, June 1985, pp. 509-515.
[6]Glauert, H., "Airplane Propellers," *Aerodynamic Theory*, Div. L., Vol. 4, edited by W. Durand, Peter Smith, Gloucester, MA, 1976, pp. 255-258.
[7]Rizk, M. H. and Jou, W.-H., "Propeller Design by Optimization," AIAA Paper 86-0081, Jan. 1986.

Modification of the Karman-Vortex Street in the Freestream

Wesley L. Goodman*
NASA Langley Research Center, Hampton, Virginia

Nomenclature

c = chord of thin flat plate
d = diameter of cylinder
E = plate eccentricity with respect to cylinder
h = gap between cylinder and adjacent plate
t = flat-plate thickness
U = freestream velocity
$U'_\infty/\bar{U}_\infty$ = freestream turbulence intensity

Introduction

OVER the past 20 years, the observation and study of "coherent structures" in turbulent shear flows (see, for example, Ref. 1) has raised the interesting possibility of turbulence control through alteration of such structures.[2] One method of providing such control is through the use of control vortices produced by embedded fixed bodies.[3] An example of the obvious success of such an approach, which is of particular interest in this Note, is Ref. 4, where a transverse cylinder mounted parallel to the wall and normal to the flow was employed to shed a Karman-vortex street which, in spite of the attendant cylinder momentum deficit, managed to "excite" or "energize" the turbulence and provide separation control/delay. Obviously, multiple as well as single bodies can be used for the production of such "control flows."[5]

The present study arose from three previous observations: 1) most of the fluctuating vorticity in a turbulent boundary layer is biased by and, hence, has the same sign as the mean velocity; 2) the influence of a nearby wall upon the Karman shedding of a circular cylinder is to suppress the portion of the street which emanates from the wall vicinity[6-13]; and 3) a collision of two shear layers of opposite sense forced to come into contact results in "pair annihilation" of the vortical layers.[11-13] The usual effect of the second observation would be to augment the first; i.e., for a transverse cylinder near a wall the shed vorticity has the same sign as the mean vorticity in the boundary layer. If the shed vorticity was of the opposite sense to that of the mean velocity, it could possibly be used as a control to diminish the vorticity within the boundary layer. The reason for producing vorticity of opposite sign is given in Ref. 14: "The only means of decay or loss of vorticity is by cross-diffusion and annihilation of vorticity of opposite signs." The purpose of this Note is to document that such single-signed Karman streets can be produced in the freestream with a relatively small flat plate (as opposed to the extensive surface employed in previous works) combined with a transverse cylinder.

Received July 15, 1985; revision received Dec. 24, 1985.

*Aerospace Engineer, Viscous Flow Branch, High-Speed Aerodynamics Division. Member AIAA.

Apparatus and Tunnel Conditions

Experimental work was conducted in the 15-in. Low-Turbulence Wind Tunnel of the Viscous Flow Branch, High-Speed Aerodynamics Division, NASA Langley Research Center. This facility operates in an open-loop mode and is capable of producing a maximum flow velocity of approximately 50 m/s.

The test section of this facility has a total length of 274 cm and a nominal 38.1 cm square cross section. The freestream turbulence intensity level was $U'_\infty/\bar{U}_\infty \simeq 0.03\%$.

The tests consisted of placing a cylinder halfway between the floor and ceiling of the tunnel, across the span of the tunnel, and normal to the incoming flow. A vertical smoke wire was positioned 8 cm upstream of the cylinder. This smoke wire consisted of a very small-diameter metallic wire that could be drawn through an oil reservoir in order to coat it with a number of evenly spaced, very small drops of oil. When a sufficient current is applied to the wire the oil vaporizes and a streakline is produced for each drop of oil (for an in-depth description, see Ref. 15). Instantaneous photographs of the streakline patterns downstream of the cylinder were acquired by use of a high-intensity strobe light/high-speed camera arrangement.

A thin plate was then stretched across the span of the tunnel in the vicinity of the cylinder. In order to minimize resonant vibrations of the thin plate, an aluminum girder framework was constructed around the tunnel to hold the plate in tension. This framework was adjustable so that the angle of attack of the plate could be zeroed, and its relative position with respect to the cylinder could be changed.

Results and Discussion

The geometrical dimensions of the cylinder and adjacent plate were varied over an extensive parameter space (see Fig. 1). The cylinder diameter was varied from 3.175 to 6.350 mm. The adjacent flat plate had a chord length that ranged from 12.7 to 25.4 mm and a thickness ranging from 0.076 to 0.965 mm. The vertical spacing between the cylinder and the adjacent plate was varied from 1.600 to 3.912 mm. The center of the cylinder was traversed ±4.7625 mm from the center of the flat plate. The optimum configuration shown in Figs. 2b and 3 consisted of a cylinder with a diameter of 4.7625 mm and a 0.254-mm-thick adjacent plate with a chord of 2.54 cm. The vertical spacing between the cylinder and the adjacent plate was 2.39 mm; with the cylinder centered below the plate.

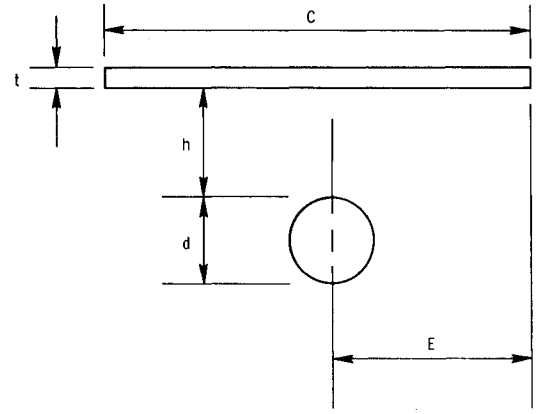

Fig. 1 Device geometry.